BRAIN
ORIGINAL ARTICLE

Local neuronal excitation and global inhibition during epileptic fast ripples in humans

Jonathan Curot,[1,2,3,4] Emmanuel Barbeau,[3,4] Elodie Despouy,[3] Marie Denuelle,[2,3] Jean Christophe Sol,[2,4,5] Jean-Albert Lotterie,[2,5] Luc Valton[2,3] and Adrien Peyrache[1]

Understanding the neuronal basis of epileptic activity is a major challenge in neurology. Cellular integration into larger scale networks is all the more challenging. In the local field potential, interictal epileptic discharges can be associated with fast ripples (200–600 Hz), which are a promising marker of the epileptogenic zone. Yet, how neuronal populations in the epileptogenic zone and in healthy tissue are affected by fast ripples remain unclear. Here, we used a novel 'hybrid' macro–micro depth electrode in nine drug-resistant epileptic patients, combining classic depth recording of local field potentials (macro-contacts) and two or three tetrodes (four micro-wires bundled together) enabling up to 15 neurons in local circuits to be simultaneously recorded. We characterized neuronal responses (190 single units) with the timing of fast ripples (2233 fast ripples) on the same hybrid and other electrodes that target other brain regions. Micro-wire recordings reveal signals that are not visible on macro-contacts. While fast ripples detected on the closest macro-contact to the tetrodes were always associated with fast ripples on the tetrodes, 82% of fast ripples detected on tetrodes were associated with detectable fast ripples on the nearest macro-contact. Moreover, neuronal recordings were taken in and outside the epileptogenic zone of implanted epileptic subjects and they revealed an interlay of excitation and inhibition across anatomical scales. While fast ripples were associated with increased neuronal activity in very local circuits only, they were followed by inhibition in large-scale networks (beyond the epileptogenic zone, even in healthy cortex). Neuronal responses to fast ripples were homogeneous in local networks but differed across brain areas. Similarly, post-fast ripple inhibition varied across recording locations and subjects and was shorter than typical inter-fast ripple intervals, suggesting that this inhibition is a fundamental refractory process for the networks. These findings demonstrate that fast ripples engage local and global networks, including healthy tissue, and point to network features that pave the way for new diagnostic and therapeutic strategies. They also reveal how even localized pathological brain dynamics can affect a broad range of cognitive functions.

1 Montreal Neurological Institute, Department of Neurology and Neurosurgery, McGill University, 3810 University Street, Montreal, Quebec, Canada
2 Departments of Neurology and Neurosurgery, Toulouse University Hospital, Toulouse, France
3 Brain and Cognition Research Center (CerCo), Centre National de la Recherche Scientifique, UMR5549, Toulouse, France
4 Faculty of Health, University of Toulouse, Paul Sabatier University, Toulouse, France
5 Toulouse Neuro Imaging Center (ToNIC), INSERM, U1214, Toulouse, France

Correspondence to: Jonathan Curot, MD, PhD
CerCo CNRS UMR 5549, Université Toulouse III
CHU Purpan, Pavillon Baudot, 31052 Toulouse Cedex, France
E-mail: jonathan.curot@cnrs.fr

Received February 09, 2022. Revised July 01, 2022. Accepted August 01, 2022. Advance access publication September 12, 2022

Correspondence may also be addressed to: Adrien Peyrache, PhD
Montreal Neurological Institute
Department of Neurology and Neurosurgery
McGill University, 3810 University Street
Montreal, Quebec, Canada
E-mail: adrien.peyrache@mcgill.ca

Keywords: epilepsy; tetrodes; micro-electrodes; high frequency oscillations; single unit

Introduction

Epilepsy is characterized by an alteration of brain dynamics. Outside of seizures, pathological signals in the local field potential (LFP) take the form of interictal epileptic discharge (IEDs). These altered neuronal dynamics are linked to cognitive impairment commonly observed in epilepsy.[1–6] IEDs are usually recorded close to the epileptogenic zone (EZ), but they can also be detected in most remote areas.[7] Such properties do not allow perfect superposition of the territories of IED recording on those that are primarily involved in the onset of seizures. However, IEDs may be associated with fast ripples (FRs)[8–10] and FRs are generally considered to be more focal than IEDs alone.[11–13] Consequently, FRs are promising candidates for an interictal biomarker of the EZ.[8,9,13–16] Unveiling the neuronal basis of FRs has therefore become a major challenge in neurology to determine the origin of the pathological dynamics and the associated cognitive impairment in epilepsy.

Epileptic patients who suffer from a drug-resistant form of epilepsy may require surgical intervention to stop, or at least diminish, the occurrence of seizures.[17] When a specific EZ is considered to be removable by surgery,[18] stereo-EEG (SEEG) is sometimes performed to determine where and how seizures begin.[7] While the recording of spontaneous seizures remains the gold standard to define the EZ, this procedure is time consuming, logistically demanding and uncomfortable for patients. These limitations could potentially be overcome by analysing the interictal periods, in particular FRs. In support of this view, resecting areas with the highest rate of FRs has been linked to a better surgical outcome.[14,19–22] The specificity of FRs in identifying the EZ was recently questioned.[23,24] However, these conclusions were drawn from observations of FRs on macro-electrodes and, overall, the study of FRs on micro-electrodes remains limited.[8,25–29]

Animal work has provided a wealth of data regarding the generation of FRs and hippocampal ripples (100–200 Hz),[2,30–37] the latter occurring in healthy tissue. This was achieved in part with techniques such as multi-channel electrophysiology, through which the activity of populations of neurons can be monitored. In humans, neuronal recordings are acquired in deep structures with single micro-wires, offering only limited separation power of neuronal waveforms, or on the cortical surface with electrode arrays that are usually distant from the EZ.[38] While previous work on the relationship between IEDs and neuronal activity reported highly diverse responses,[39–41] the specificity of local and long-range population responses of FRs remains unclear. Here, we used a new type of intracranial electrode equipped with micro-wires bundled in tetrode configurations.[42] Tetrodes (composed of four micro-wires bundled together) provide a high yield in the number of isolated units[43,44] and a much higher spatial resolution to localize the source of FR generators. As these micro-wires are guided through regular intracerebral depth electrodes routinely used for the localization of the EZ, FRs can be recorded at both micro and macro levels simultaneously, with high spatial correspondence in relation to neuronal activity.

In this study, interictal FRs were detected in subjects implanted with these new 'hybrid' electrodes. We first demonstrate that FRs are associated with high neuronal excitability in the EZ. Next, we show that neurons outside the EZ are not excited by FRs, yet they decrease firing after FRs. Last, we show that the decrease in post-FR firing can last up to 1 s and is related to the inter-FR intervals. We suggest that this global post-FR inhibition is part of a refractory mechanism that prevents FRs from developing into prolonged ictal discharges.

Materials and methods

Population and surgery

The epileptic patients underwent SEEG[45] in the Neurophysiological Explorations unit in Toulouse, between September 2015 (Subject 1) and November 2019 (Subject 9). Patient consent was obtained according to the Declaration of Helsinki and all experiments and analyses were approved by the local ethics committee and the French Drug and Health Products Safety Agency (CPP Sud-Ouest et Outre-Mer I ethical board, no. 1-14-23, and ANSM 2014-A00747-40). All subjects suffered from focal epilepsy and antiseizure drugs failed. The precise location of the EZ could not be specified by non-invasive assessments in all patients (including MRI, video-EEG, functional imagery, such as 18-FDG PET in all patients, and additional ictal single photon emission CT in some patients). Epilepsy lesions and the aetiologies of epilepsy were heterogeneous across patients (Table 1). SEEG recordings were performed to accurately define the EZ and as part of the patients' clinical care. The antiseizure drug was gradually reduced to facilitate seizure occurrence for several days following each implantation, according to the usual clinical procedure. Each subject received detailed information about the objectives of the SEEG before intracerebral electrode implantation and about the use of hybrid electrodes. They signed an informed consent form for the implantation and use of the EEG data for research purposes. The new hybrid macro–micro-electrodes (DIXI Medical; maximum of four per subject) were implanted.[42,46]

Electrodes

SEEG recordings were taken using intracerebral multiple-contact depth electrodes implanted intracranially according to Talairach's stereotactic method.[47] The location of each electrode contact was based on the co-registration of postoperative CT scan/preoperative 3D T_1-weighted MRI data. The resolution of these data fusions enables visual verification of the anatomical location of each contact and its location in grey or white matter. The choice of electrode location was based solely on pre-SEEG clinical observations and on hypotheses about the location of the EZ based on non-invasive

Table 1 Patients' clinical characteristics, location of hybrids and yield of neurons and FRs per tetrode

Subject sex/age	Hybrid name	Tetrodes	Neurons (*n*[a])	FRs (*n*)	Anatomical location	Location related to epileptic network	Lesion type	Surgical decision	Outcome[b]
1	a	a1, a2, a3	0, 3, 3	0	Amygdala, R	IZ	Hippocampal sclerosis	L ant. temporal lobectomy (ap, bp, tbp included)	Engel 1a ILAE 1
M/41 y	bp	bp1, bp2	0, 0	139	Ant. hippocampus, L	EZ			
	ap	ap1, ap2, ap3	7, 2, 2	129	Amygdala, L	EZ			
	tbp	tbp1, tbp2	0, 0	281	Rhinal cortex, L	EZ			
2	tb	tb1, tb2	0, 0	0	Rhinal cortex, R	IZ	Encephalitis sequelae	L ant. temporal lobectomy (ap, cp, tbp included)	Engel 3a ILAE 4
M/55 y	cp	cp1, cp2, cp3	4, 7, 0	430	Post. hippocampus, L	EZ			
	ap	ap1, ap2	0, 0	74	Amygdala, L	EZ			
	tbp	tbp1, tbp2	3, 9	42	Rhinal cortex, L	EZ			
3	a	a1, a2	0, 0	13	Amygdala, R	IZ	Hippocampal sclerosis	L ant. temporal lobectomy (tpp, ap, cp, tbp)	Engel 2b ILAE 3
M/44 y	tpp	tpp1, tpp2,	0, 0	0	Temporal pole, L	EZ			
	ap	ap1, ap2	0, 0	24	Amygdala, L	IZ			
	cp	cp1, cp2	1, 1	4	Post. hippocampus, L	IZ			
4	gl	gl1, gl2	2, 3	0	Lingual gyrus, R	O	Cortical dysplasia	L ant. temporal lobectomy (tpp, ap, cp, tbp)	Engel 1a ILAE 1
F/36 y	glp	glp1, glp2	0, 4	0	Lingual gyrus, L	O			
	otp	otp1, otp2	0, 0	0	Fusiform gyrus, L	IZ			
	tbp	tbp1, tbp2, tbp3	0, 3, 0	23	Rhinal cortex, L	EZ			
5	h	h1, h2	0, 8	0	STG, R	IZ	Hippocampal sclerosis, cortical dysplasia	R ant. temporal lobectomy (b included)	Engel 1a ILAE 1
M/16 y	b	b1, b2	0, 0	30	Ant. hippocampus, R	EZ			
	ot	ot1, ot2	0, 0	0	Fusiform gyrus, R	IZ			
	cp	cp1, cp2	0, 0	0	Post. hippocampus, L	O			
6	tbp	tbp1, tbp2	0, 0	4	Amygdala, L	IZ	Cortical development abnormality	NA (waiting for another SEEG)	NA
M/58 y	b	b1, b2	0, 0	0	Ant. hippocampus, R	O			
	bp	bp1, bp2	0, 0	286	Ant. hippocampus, L	IZ			
	tpp	tpp1, tpp2	0, 0	0	Temporal pole, L	IZ			
7	tb	tb1, tb2	0, 8	0	Rhinal cortex, R	IZ	Meningo-encephalocele	Contraindication	NA
M/54 y	tpp	tpp1, tpp2	15, 2	0	Temporal pole, L	EZ			
	cp	cp1, cp2, cp3	0, 0, 0	26	Post. hippocampus, L	EZ			
	tbp	tbp1, tbp2	0, 1	0	Rhinal cortex, L	EZ			
8	b	b1, b2, b3	0, 4, 12	93	Ant. hippocampus, R	EZ	Hippocampal sclerosis	R ant. temporal lobectomy (b, c included)	Engel 1a ILAE 1
F/49 y	c	c1, c2, c3	0, 0, 4	63	Post. hippocampus, R	EZ			
	bp	bp1, bp2	0, 4	13	Ant. hippocampus, L	IZ			
9	fca	fca1, fca2	5, 0	18	Post. medial temporal, R (within nodular heterotopia)	EZ	Nodular heterotopia	Contraindication, thermocoagulation of heterotopia planned (fca included)	NA
M/26 y	a	a1, a2, a3	5, 0, 9	71	Amygdala, R	IZ			
	tb	tb1, tb2	0, 0	0	Rhinal cortex, L	IZ			
	ap	ap1, ap2	4, 2	0	Amygdala, L	IZ			

Further information is provided in the Supplementary material. Ant. = anterior; EZ = epileptogenic zone; F = female; IZ = irritative zone; L = left; M = male; MNI space origin (x = 91, y = 126, z = 72); NA = not applicable; O = healthy tissue; Post. = posterior; R = right; STG = superior temporal gyrus.

[a]Per tetrode, respectively.

[b]Outcome according to ILAE and Engel Classifications.

assessment. The global electrode plan was specific for each patient and combined semirigid multi-lead clinical depth macroelectrodes (Microdeep, DIXI Medical) and hybrid electrodes. The macroelectrodes had a diameter of 0.8 mm and contained 5–18 contacts (platinum/iridium) 2 mm long and 1.5 mm apart. Two to four hybrid electrodes were implanted per subject depending on clinical and anatomical constraints (e.g. intra-parenchymal length versus available length of electrodes). The hybrid electrodes are similar in design to regular depth electrodes (diameter 0.8 mm, length 33.2, 40.4 or 50.8 mm, depending on the configuration, 6–9 macro-contacts) and equipped with two or three tetrodes (four micro-electrodes each) that protruded 3 mm from the shaft between the first and second most medial macro-contacts. Each tetrode is made by twisting four micro-wires (tungsten, 20 µm) together and connecting them to a specific connector. The tetrodes are extruded by rotating an external micrometre screw immediately after implantation in the operating theatre. In this study, tetrodes were all located between the first two macro-contacts (from the tip of the depth electrode).

Recording system

Macro-contact signals were recorded using two SystemPLUS EVOLUTION 64-channel acquisition units (Micromed) at a sampling rate of 2048 Hz (anti-aliasing filter 926.7 Hz; high-pass filter 0.15 Hz; low-pass filter 1000 Hz). We used the raw SystemPLUS signal to avoid unnecessary filtering.[48] Simultaneously, microelectrode signals were continuously acquired using a 64-channel Cerebus System amplifier (Blackrock Microsystems) at a sampling rate of 30 kHz (0.3–7.5 kHz bandwidth) and time synchronized with the macro-contact signal. Line noise cancellation at 50 Hz was applied. A macro-contact located in white matter was chosen as a reference for both systems. Macro-contacts were recorded for 24/24 hours. Micro-electrodes were recorded for 1 h in five morning sessions, while the subject watched television.

Spike sorting

Raw electrophysiological recordings were preprocessed within the Brainstorm environment.[49] Semi-automatic spike sorting was done offline on each separate tetrode using SpyKING CIRCUS with a template matching-based algorithm[50] on a 1-h signal. Different quality metrics were considered: inter-spike interval, scatterplots of the different clusters, amplitude over time, auto-correlogram, cross-correlogram and refractory period violations to optimize spike sorting.[51] An action potential was detected if the amplitude was above a threshold set at six times the median of the absolute deviation of the voltage. The resulting data were followed by manual data curation in Klusters software.[52]

Fast ripple detection

Thirty-four subjects were included in the global EpiFar project during the inclusion period. A preselection of EEG data for further coupled FRs and neuronal analyses was based both on the results of the spike sorting (see next) and on those of the FR detection on 10-min samples on Days 3 and 4 after implantation in these 34 subjects. The selection of subjects in the current research was based on (i) the quality of EEG signal that could be unanalysable in some cases due to a low signal-to-noise ratio; (ii) FR visualization on a 10-min signal sample during preselection; and (iii) visible neuronal activity with the possibility of clustering. Depending on these criteria, we selected 1 h of recording in nine subjects, which consisted of 26 hybrids for further neuronal and FR analyses.

Visual analysis of high frequency oscillations is still considered the gold standard for their assessment.[23,53] However, visual analysis might be subjective and is highly time consuming. On the contrary, automatic detectors have highly heterogeneous performances and none have been validated on human tetrode recordings. Therefore, we decided to combine automatic detection of FRs and visual analysis.[46] FRs were visually and automatically analysed during 10-min epochs in each subject on the third and fourth days of recording during the waking period. This duration of sample recordings is at least similar or even longer than in previous publications.[23,53] We deliberately chose a duration of analysis over 2 days since the FR rate can be highly variable from one day to the next, especially in relation to the progressive withdrawal of treatment. In most cases, on the third and fourth days subjects' antiseizure drug was reduced. In parallel, this FR detection for preselection was training to improve manual isolation of FRs on a longer signal duration for further analyses. There were three criteria for identifying FRs: (i) visible oscillation in both the raw data and the filtered signal (200–600 Hz finite impulse response bandpass filter to reduce ringing); (ii) at least four oscillations with an amplitude clearly higher than the baseline[54]; and (iii) time-frequency analysis resulting in circumscribed areas in the time-frequency plane in the FR band to avoid artefacts and false ripples created by filtering.[48,55] Monopolar montages and reformatted bipolar montages were used for micro- and macroelectrode recordings, respectively. First, we used the automatic detector Delphos[56] in the Anywave software[57] on all 10-min epochs. This is an automatic detector that improves the detectability of high-frequency oscillations by applying linear whitening (i.e. flattening) transformation to enhance fast oscillations while preserving an optimal signal-to-noise ratio. Each event detected by Delphos was then manually reviewed to verify whether all previous criteria were met. The raw and filtered signals (200–600 Hz) of the four micro-wires of each tetrode were visualized simultaneously using a 0.6 s time window. FRs were detected independently by two researchers (J.C., E.D.), blind to clinical conclusions and healthy regions, as well as to the final decision regarding neurosurgery at the moment of FR detection. Events without the three previous criteria were systematically rejected. Noisy periods or channels were excluded. In the nine subjects selected, FRs were then manually tracked in Brainstorm[58] on a 1-h signal on the micro-electrodes (see criteria for identification next).

We calculated two different indices to characterize the FRs: spectral mode (i.e. frequency peak) and entropy.[59,60] These indices were calculated from the power spectral density, which is an estimate of the power distribution at which the frequencies that make up the signal are expressed. Entropy measures the monotonicity of the frequency spectrum.

Determination of the epileptic network

In clinical practice, the EZ is an electroclinical definition that corresponds to the networks of brain regions that generate seizures.[61,62] The complete removal of the EZ is essential to prevent seizures after surgery.[17] EZ should integrate the seizure-onset zone. The irritative zone (IZ) is the IED site.[7,63,64] The propagation zone refers to brain areas where delayed secondary electrophysiological discharges are observed outside the EZ. Healthy brain tissue (O) are the areas with no EZ and IZ overlap and where no seizure is propagated. The clinical EZ and non-EZ as well as the IZ, propagation zone and healthy areas were independently determined by the

clinical team of epileptologists after reviewing the clinical iEEG data (L.V., M.D.). They were blind to FRs and neuronal analyses. All the neuronal and FR analyses were primarily done by J.C. and A.P., who were blind to final clinical conclusions.

Motion tracking

Each subject's movement during recording was tracked on a single video camera (at 25 Hz) and the acquisition was synchronized with electrophysiological data (Micromed) in three subjects (1, 6 and 8). Videos were processed *post hoc* using Deeplabcut[65] to analyse subjects' movements (Fig. 1). In each subject, six points were tracked: nose, chin, left/right shoulders and left/right hands. A Resnet50 network was trained for at least 100 000 iterations or longer if tracking was not satisfactory. The velocity of each marker was computed and smoothed with a 1-s Gaussian kernel. The velocity for time stamps at which the log-likelihood of marker detection was below 0.95 was considered null. Overall movement velocity was computed as the average velocity of all markers. Subjects were considered still if the average marker velocity was below 25 pixels/s for at least 3 s.

Computing and comparison of Z-scored cross-correlograms

Cross-correlograms were computed between FRs (or IED in Supplementary Fig. 3) and individual spike trains in bins of 10 ms and ±10 s at around the time of the events. Cross-correlograms reflect the average firing rate of a neuron relative to the timing of FRs, and are therefore biased by the neuron's firing rates. To normalize fluctuation and compare neurons of different firing rates, cross-correlograms were Z-scored following a three-step procedure, as described by Viejo *et al.*[66] (Supplementary Fig. 2). First, cross-correlograms were convolved with a Gaussian kernel of 1-s SD. This provides expected cross-correlograms for modulation slower than 1 s (e.g. brain states). Next, cross-correlogams were convolved with a Gaussian kernel of 40-ms SD. This step smooths bin-to-bin variability mostly resulting from limited sampling. Last, cross-correlograms were Z-scored. To this end, we assumed that spike trains are Poisson processes. The SD of the firing rate at any point in the cross-correlograms is then equal to the square root of the firing rate. The Z-scored cross-correlograms are defined as the difference between the observed and expected cross-correlograms divided by the square root of the expected cross-correlograms.

To evaluate similarities and differences in temporal profiles of neuronal modulation around the time of FRs, we first transformed the cross-correlograms with a non-linear function (Arctan) so that the main effect was not dominated by differences in absolute activation. We then projected the transformed cross-correlograms on the first two principal components of the cross-correlograms (accounting for ~90% of the total variance). Finally, for each neuron, we computed their Mahalanobis distance to all other neurons of the same tetrode and of the other tetrode of the same hybrid electrode, and/or the mean distance to tetrodes of other hybrid electrodes of the same subject.

Computing IED spike-and-wave duration

To test the relationship between neuronal modulation by FRs and the shape of the spike-and-wave event in the LFP, we determined the typical duration of the LFP event independent of its polarity or potential multi-phasic nature (Fig. 6). To this end, we computed the spectrogram of the average FR-triggered LFP in the same window as spikes (–0.3–2 s). The inverse of the frequency with the highest power was defined as the typical duration of the event.

Data availability

All data supporting the findings of this study will be made available to the public before publication. Any code related to the analyses of the manuscript will be made available to the public before publication.

Results

Drug-refractory epileptic patients ($n = 9$; Table 1) were implanted with 8–15 depth electrodes to accurately localize the EZ. Following implantation, SEEG recordings were made for 5 to 12 days. Our analysis epochs were extracted from the first 5 days.

A new macro–micro electrode for multi-scale neuronal analyses

We used a new device to simultaneously record LFPs and multiple single units in deep local brain circuits. Three to four of the implanted depth electrodes were a hybrid version that combines macro-contacts and 2–3 tetrodes between the two deepest macro-contacts (8–12 tetrodes per subject; see 'Materials and methods' section). LFPs were recorded for 1 h at a high sampling rate (30 kHz) in each subject during the day-time period. FRs (200–600 Hz) were visually detected throughout this 1-h signal.[13,46]

We selected nine subjects (clinical details in Table 1) from our entire database who met all the following requirements: a high signal-to-noise ratio, detection of at least one FR and/or detection of at least one isolated single unit on one tetrode. Tetrode locations were confirmed by co-registration of preoperative stereotactic MRI and postoperative CT scans (Fig. 1A), and the dataset was composed of recordings in the anterior hippocampus (nine hybrid electrodes, 21 tetrodes), posterior hippocampus (6, 15), amygdala (8, 19), rhinal cortex (8, 17), temporo-occipital or lingual gyrus (6, 12), temporal pole (3, 6) and superior temporal gyrus (2, 4). Thirty-seven tetrodes were located in the right hemisphere, 49 in the left hemisphere. Both FRs and single units were recorded on 16 tetrodes, FRs only on 31 tetrodes, and action potentials only (without any FRs) on 12 tetrodes (Fig. 1B). A total of 2233 FRs were detected in the nine subjects (4–470 FRs per hybrid electrodes). We further validated the pathological nature of the FRs detected. They have the following features: median spectral mode 304 ± 28 Hz and median entropy 5.8 ± 0.4 (Supplementary Fig. 1).

It is important to note that all FRs were associated with an IED (see, for example, Fig. 1C–D), which demonstrates that they were not simply physiological ripples. FRs were generally very similar on all four wires of a tetrode. However, FRs often had different amplitudes and were not necessarily in phase on the different tetrodes of the same hybrid electrode (Fig. 1D). Because the tetrode tips of a hybrid electrode are separated by at most 2 mm,[42] these findings suggest that the underlying neuronal generators of FRs are characterized by an anatomical scale in the millimetre range.

Micro-wire recordings reveal signals that are not visible on macro-contacts. In fact, FRs detected on the deepest macro-contact (that is, the closest to the tetrodes) were always associated with FRs on the tetrodes. However, the opposite was not always true: 82% (range 38–100%) of the FRs detected on tetrodes were associated with detectable FRs on the nearest

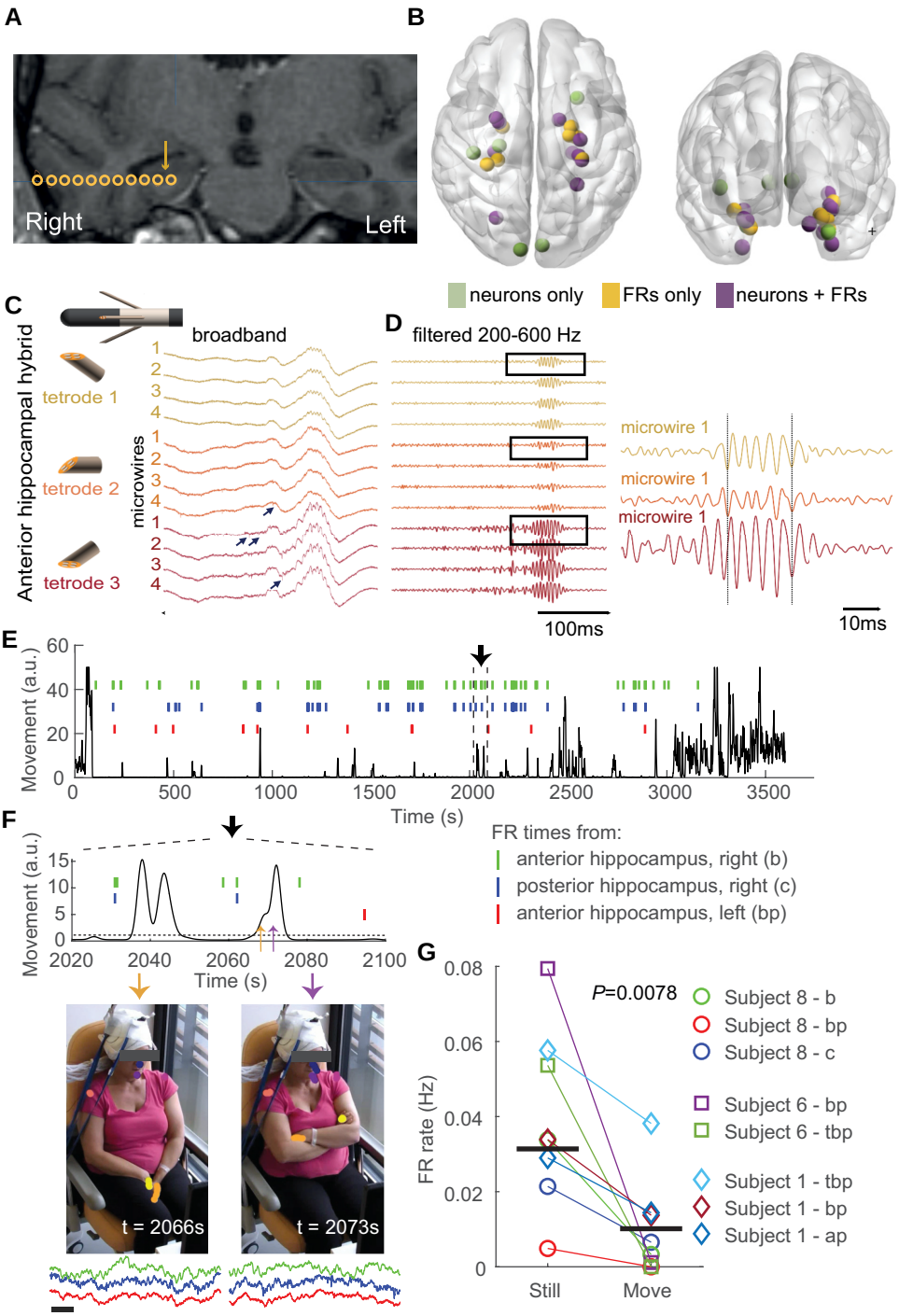

Figure 1 Recording of intracerebral signals with micro-wires at a high sampling rate reveals local FRs and action potentials. (**A**) Example of a hybrid electrode location in one subject (Subject 8). Coronal co-registration MRI CT scan (preoperative 3D T_1 MRI with gadolinium and postoperative CT scan). Circles are macro-contacts; the arrow specifies the putative location of tetrodes between the two deepest macro-contacts of the hybrid electrode. (**B**) Locations of every tetrode included in the study, referenced in the MNI space. Colours indicate whether FRs, single units (neurons) or both were detected. See Table 1 for complete list of locations. (**C**) Schematic representation of the deepest macro-contacts and the three tetrodes and example LFP traces (broadband) from the three tetrodes of a hybrid electrode targeting the right anterior hippocampus (Subject 8). The IED (positive deflection) is associated with an FR. Note that both IED and FR amplitude are higher on the third tetrode. Black arrows indicate action potentials. (**D**) *Left*, Same signals as in **C** filtered in the FR frequency band (200–600 Hz). Note that FRs have the same morphological features on the four micro-wires of each tetrode. *Right*, Zoomed trace of the first micro-wire of each tetrode. Although FRs occur at the same time, moment-to-moment phase difference varies. (**E**) Subject's upper body movement (see 'Materials and methods' section) and occurrence times of FRs on three hybrid electrodes during a 1-h long recording. (**F**) *Top*, Temporal zoom of the traces in **E** (delimited by vertical dotted lines). *Bottom*, Two video frames extracted at times indicated by the orange and purple arrows in the *top* panel. Note the markers on the head, shoulders and hands. Examples of micro-wire recordings from the three depth electrodes showing FRs, centred around the time of video frame, are shown below (same colour ticks depicting FR times). Scale bar = 100 ms. (**G**) FR occurrence rate during stillness and movement for all three subjects with video tracking. Horizontal bars indicate median values.

macro-contact ($n = 6$ hybrid electrodes in three subjects with synchronized macro-contact and tetrode recordings). These numbers are only illustrative of the current dataset and at this point do not necessarily indicate that micro-electrodes have a higher reliability in detecting FRs. However, this observation is additional evidence that FR generators can be smaller than the volume of tissue that typically influences the electrical signals on macro-contacts.

Variations in FRs on micro-wires depend on vigilance state

The occurrence rate of FRs recorded on clinical macroelectrodes depends on vigilance states, showing the highest incidence during sleep.[22] Here, we asked whether FRs detected on micro-wires were also modulated by vigilance states at a fine temporal resolution. To this end, we recorded subjects with a camera. The video stream of the camera was synchronized with the tetrode electrophysiological signals in three subjects with a high FR incidence rate on at least two hybrid electrodes (see Methods section). While the recordings only included the interictal day-time period in the morning, these three subjects all showed a highly variable level of attention during the recording, from fully awake to asleep. We determined their vigilance states by tracking their movements using DeepLabCut[65] (see 'Materials and methods' section) (Fig. 1E–F). Movement electrical artefacts can decrease the sensitivity of FR detection, leading to a spurious decrease in FR rate. However, artefacts were virtually absent in these recordings, as shown in the example subject (Fig. 1F). We observed a 3-fold increase of the FR occurrence rate during the immobility period ($P = 0.0078$, $n = 6$ hybrid electrodes, Wilcoxon sign rank test; Fig. 1G). These findings show that brain states corresponding to even transient motor activity are associated with a decrease in the excitability of FR generators.

FR and single unit recording in local and global circuits

Raw electrophysiological signals were processed to semi-automatically extract action potentials (Fig. 2; see 'Materials and methods' section). A total of 139 single units were isolated in nine subjects, corresponding to 17.4 (± 9.1 SD) single units per subject, 7.3 (± 5.1) per hybrid electrode and 5 (± 3.6) per tetrode (for all subjects, hybrid electrodes or tetrodes where at least one single unit was detected). The average firing rate was 1 Hz (range 0.33–2.35 Hz, 1st and 3rd quartiles).

To investigate the relationship between neuronal activity and FRs, we divided the dataset into local and global interactions, corresponding to neuronal activity in relation to FRs recorded on the same hybrid or another hybrid electrode ($n = 78$ and 190 single units studied for local and global interaction, respectively, in nine subjects; note that the same neuron could be counted twice if FRs were detected on more than one hybrid).

FRs are associated with local excitation followed by global inhibition

Next, we questioned how FRs modulated local and global neuronal activity in epileptic subjects. To address this question, we computed spike train cross-correlograms in relation to FR occurrence times (that is, average firing rate according to time-lag from FRs). Firing rates varied widely in the cortex,[67] making a direct comparison of cross-correlograms challenging. Therefore, we normalized cross-correlograms by number of standard deviations from baseline (i.e. average firing rate expected by chance) for each time lag[66] (Fig. 3A; see 'Materials and methods' section and also Supplementary Fig. 1).

At the time of FRs, local neurons, but not neurons from remote hybrid electrodes, showed high activation (Fig. 3B–D; $P = 6.6 \times 10^{-8}$, 0.81; $n = 78$, 190 for local and global interaction, respectively; Wilcoxon signed rank test; local firing greater than global firing: $P = 6.7 \times 10^{-9}$, Mann–Whitney U-test). In contrast, both the local and global networks showed a decrease in firing rates after FRs (Fig. 3B–E; $P = 5 \times 10^{-10}$, 2.2×10^{-5}; Wilcoxon signed rank test). However, the decrease in local firing rate was significantly greater than for remote neurons ($P = 1.3 \times 10^{-9}$, Mann–Whitney U-test). These observations provide additional evidence that FR generators are restricted to local circuits. Interestingly, they point to a potential mechanism to dampen activity following FRs in large-scale networks.

We then sought to determine whether the variability in neuronal responses in terms of both the activation of local neurons during FRs and local and global inhibition, could be explained by anatomical and subject-specific factors. We first examined local network responses. Most local neurons showed increased firing rates at the time of FRs (Fig. 3C–E; 57/78 neurons with $z > 0$; $P = 2 \times 10^{-5}$; binomial test) and a post-FR decrease in firing rates (64/78 neurons with $z < 0$; $P = 3 \times 10^{-9}$; binomial test). The FR increase and post-FR decrease in firing rates were correlated (Fig. 3D; $r = 0.39$; $P = 2 \times 10^{-4}$; Pearson's correlation) and, accordingly, local neurons that were activated with the FRs were virtually all followed by a period of decreased firing (51/57 neurons, $P = 3 \times 10^{-10}$; binomial test).

Next, we examined two potential sources of variability at the global level: post-FR firing rates depended neither on whether FRs were ipsi- or contra-lateral ($P = 0.3$; Kruskal–Wallis test) nor on the status of the network (EZ, IZ or healthy cortex; see 'Materials and methods' section) from which neurons were recorded (Fig. 3F; $P = 0.08$; Kruskal–Wallis test), suggesting a global phenomenon that cannot be accounted for by a simple relationship between the FR-generating tissue and the target areas.

Local homogeneity but global heterogeneity in neuronal responses to FRs

Local networks are highly activated at the time of FRs, but are all neurons similarly modulated? To address this question, we focused our analysis on three subjects in which at least one hybrid showing FRs had two tetrodes, each with at least three neurons (Fig. 4A; total of 10 tetrodes on 6 hybrid electrodes). Neuronal activation at the time of FRs was more similar within each tetrode than across tetrodes (Fig. 4B; $P = 1.4 \times 10^{-4}$; $n = 82$ neurons from $n = 4$, 3, 3 tetrodes from the same hybrids in three different subjects; Kruskal–Wallis test).

Although absolute activation visibly differs between tetrodes from the same hybrids (but generally fails to reach statistical significance because of limited sampling), the relative temporal profile of neuronal activity around FRs may still be specific to local networks. To test for this hypothesis, we first re-normalized cross-correlograms to compress the range of extreme values. We then computed the similarity (i.e. Mahalanobis distance, see 'Materials and methods' section) of each neuron to subsets of other neurons from the same or other tetrodes. In each subject, the response profile of each neuron was more similar to the other neurons of the same tetrodes than to the neurons of tetrodes of other hybrid electrodes (Fig. 4C; $P < 10^{-6}$, $n = 64$, paired t-test), but was similar to neuronal responses on tetrodes from the same hybrid electrodes

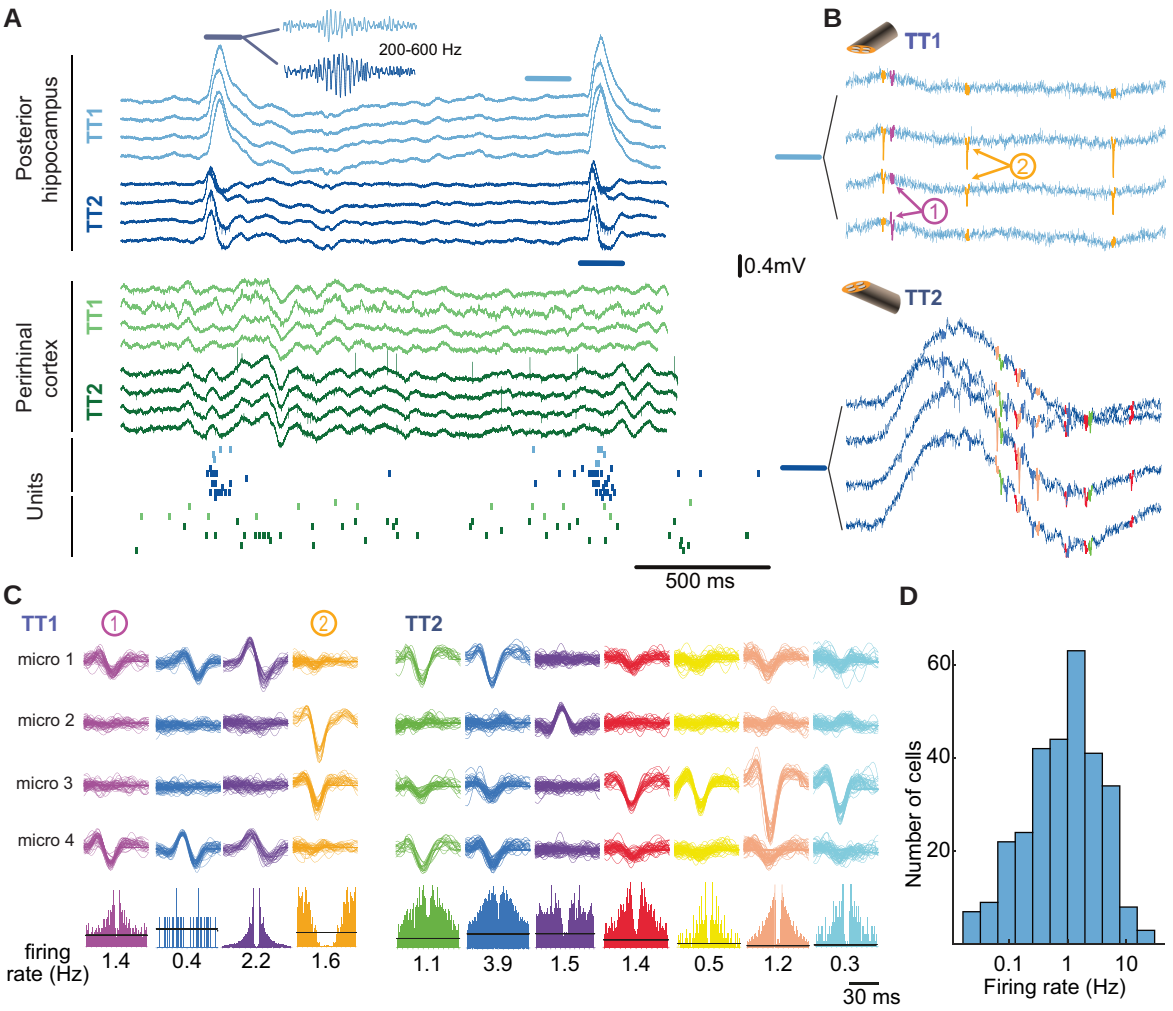

Figure 2 FR and spikes in local and global circuits. (**A**) LFP recordings (unfiltered broadband signal) on two hybrid electrodes in Subject 2. Two IEDs are visible in the posterior hippocampus, one in the perirhinal cortex. IEDs were associated with FRs, as shown in the inset (200–600 Hz filtered LFP trace). Bottom, raster plot of neuronal activity. Each row corresponds to one unit and each dot to one action potential. There is an increase in firing in most units during the IED and FR recording on TT1 and TT2 located in the posterior hippocampus (blue and purple dots). (**B**) Action potentials recorded on the posterior hippocampus on TT1 and TT2 immediately before the highlighted FR in **A** (TT1) and during the FR (TT2). Note the FR in the broadband on the TT2 trace. (**C**) Sample waveforms of action potentials recorded on TT1 and TT2 in the posterior hippocampus, sorted into putative single units. Bottom, auto-correlogram (± 30 ms) and mean firing rate of each single unit. (**D**) Distribution of single unit firing rates (log scale).

($P > 0.05$, $n = 55$, paired t-test; Fig. 4C). Overall, these observations provide further evidence for the small scale (~1 mm) of FR generators and suggest that neurons of a given brain area show similar dynamics although absolute activation may differ.

Circuit-specific post-FR recovery of neuronal activity and FRs

Post-FR inhibition is particularly high in FR-generating networks bearing strong similarities to inhibitory currents that govern hippocampal activity following physiological ripples[32,34] believed to impose a refractory period on ripple generation. Therefore, we questioned whether post-FR decrease in firing rate was related to the dynamics of FR generation. First, we characterized post-FR inhibition for each single cell by fitting a sigmoid on spike train cross-correlograms related to FRs (Fig. 5A). Post-FR neuronal recovery time was defined as the time of maximum sigmoid slope after the FR (that is, the time at which neurons reached 50% of their baseline firing rate). Only units for which the sigmoid fit converged and for which the recovery time was within the range of 50–1500 ms were included in the analysis ($n = 55$ single units).

To unravel a potential relationship between neuronal and network-level dynamics, we focused our analysis on three subjects with at least four neurons on two different tetrodes from the same hybrid showing FRs on these tetrodes (Fig. 5B). While post-FR recovery times were broadly distributed across all three recordings, from 282 ms (10th percentile) to 816 ms (90th percentile) (Fig. 5C), there was less variability within a tetrode than across tetrodes (Fig. 5D; $P = 5 \times 10^{-6}$; Kruskal–Wallis test), sometimes even on the same hybrid (see, for example, cp and tbp hybrids in subject 2). Next, we determined the typical recovery time of FRs as the median of all inter-FR intervals <10 s (Fig. 5E). We then determined the circuit-specific neuronal recovery time as the median recovery times of all neurons recorded on a given tetrode. Neuronal recovery times were of the same order of magnitude as FR recovery time and yet neuronal recovery always preceded FR recovery on a tetrode-by-tetrode basis (Fig. 5F; $P = 0.0039$, $n = 9$ tetrodes; Wilcoxon signed rank test). These findings suggest that post-FR

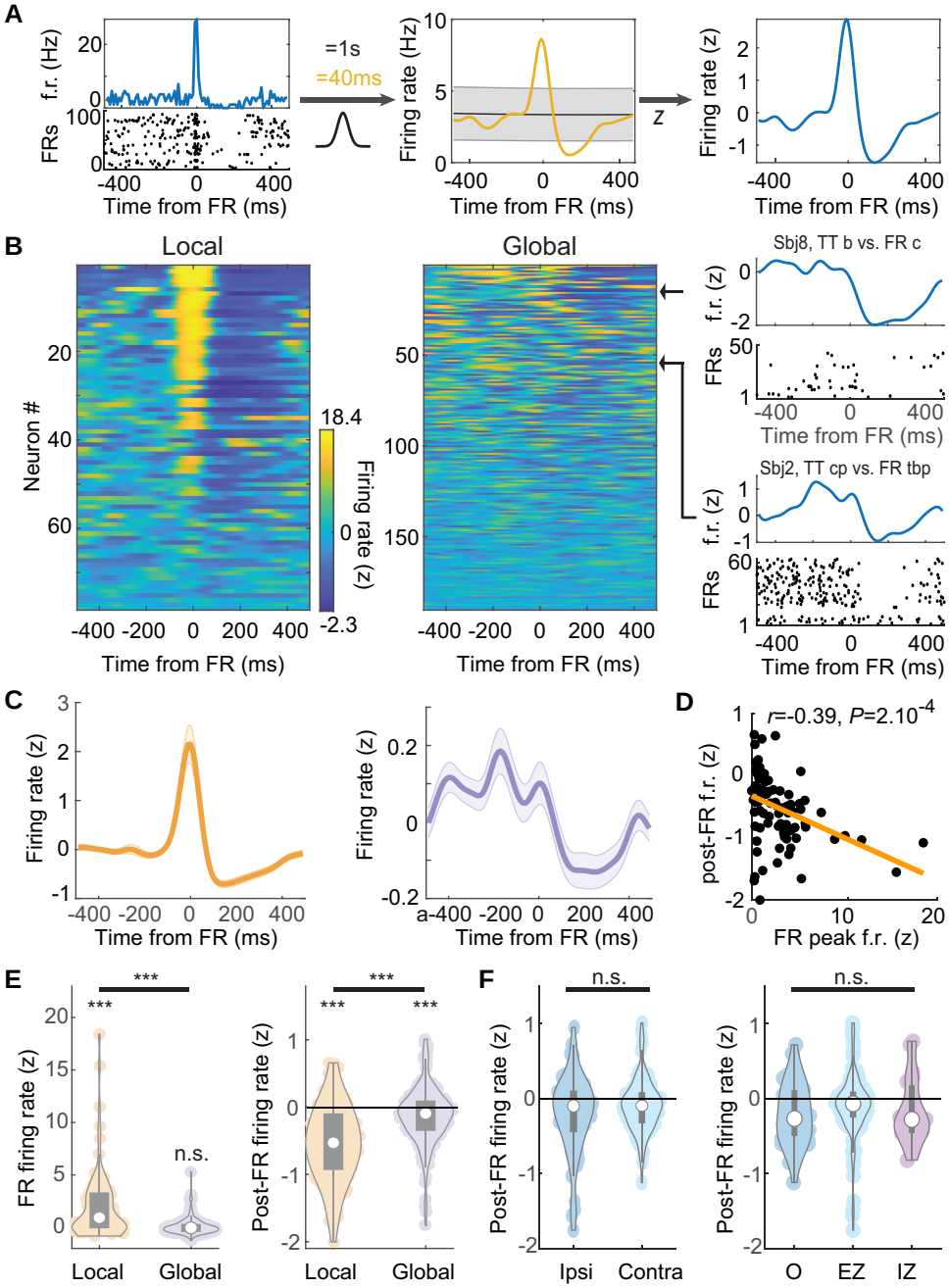

Figure 3 Local and global modulation of neuronal activity with FRs. (**A**) Normalization of a sample single unit cross-correlogram relative to time of FRs. Time 0 corresponds to the occurrence of FRs. *Left*, Mean firing rate (f.r.) of the neuron relative to FR occurrence time (*top*) and raster plot of FR-by-FR spiking activity (*bottom*); *middle*, the cross-correlogram is convolved with two Gaussian filters of different width; *right*, the Z-scored normalized firing rate (see 'Materials and methods' section). (**B**) Normalized cross-correlograms of each single unit recorded at the local (same hybrid as FR) and global scale (different hybrid) relative to FRs. Colours display Z-scored firing rates. Cross-correlograms are sorted by their overall variance, from maximum (*top*) to minimum (*bottom*). *Right*, Two sample single units at the global range (titles indicate location of hybrids from which neuron and FRs were recorded). (**C**) Average local (*left*) and the global (*right*) cross-correlograms. (**D**) Post-FR firing rates as a function of FR peak firing rates in local networks. (**E**) *Left*, FR local and global peak firing rates; *right*, same for post-FR firing rates. (**F**) *Left*, Post-FR global firing rates for ipsi- and contralaterally located hybrid electrodes (i.e. hybrids on which FRs and neurons were monitored). *Right*, Same for the different statuses of the neuron-recording hybrid electrodes (O, healthy tissue). In **E** and **F**, white circles indicate the median, and grey rectangles the distribution of the first two quartiles around the median.

neuronal inhibition is governed by circuit-specific properties and plays an important role in delaying the occurrence of the next FR, but not the rate of FRs.

Is neuronal response related to the shape of the IED in the LFP (Fig. 5B)? To address this question, we determined the duration of FR-triggered IED in a manner that is independent of both IED polarity and of potential multiphasic pattern (Fig. 6A, see 'Materials and methods' section). Remarkably, the duration of IEDs was correlated with the average neuronal recovery period (Fig. 6B, $r = 0.69$, $P = 0.028$, Pearson's correlation). In conclusion, the shape of the IED, and especially its duration, is certainly a direct consequence of post-FR neuronal inhibition.

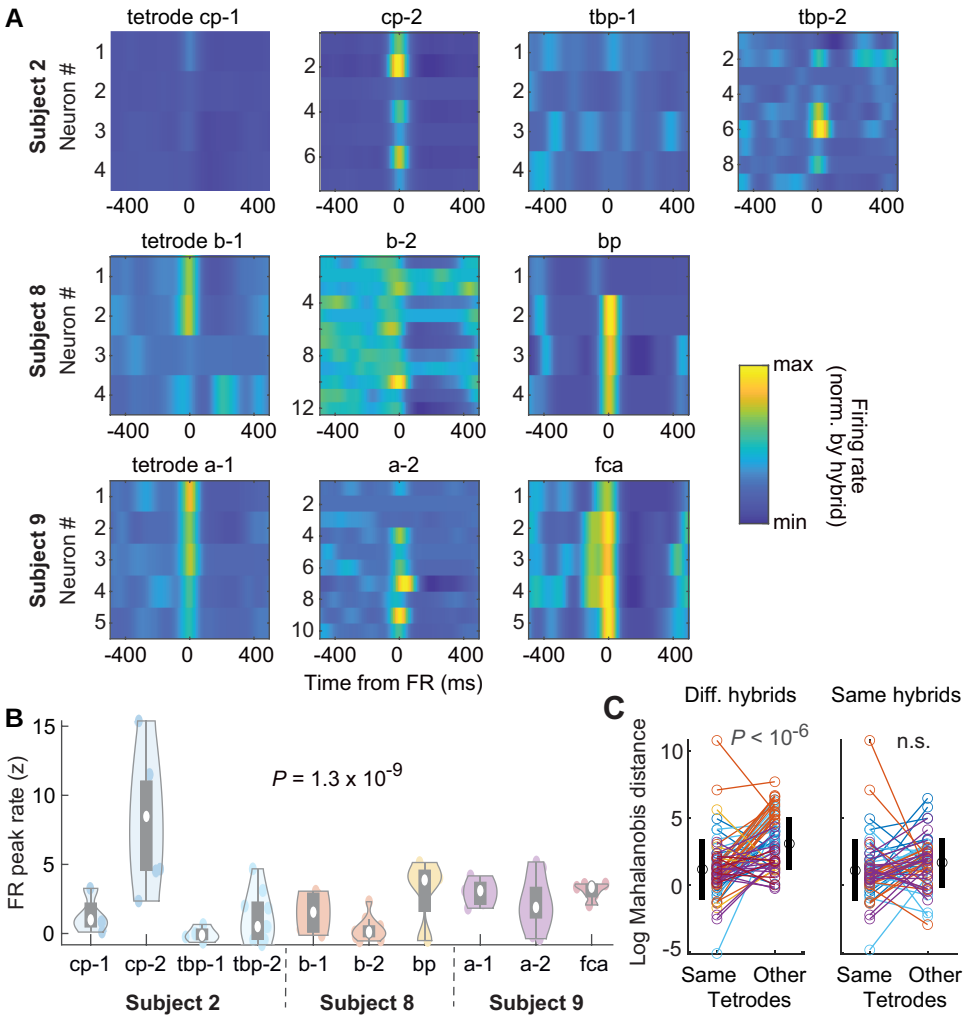

Figure 4 Neuronal modulation by FRs in local networks. (**A**) Tetrode-by-tetrode neuronal cross-correlograms in three subjects (total of 6 hybrid electrodes and 60 single units). Colour indicates *Z*-scored firing rates from minimum (blue) to maximum (yellow) on each hybrid electrode. (**B**) Distribution of tetrode-by-tetrode peak FR firing rates. White circles indicate the median and grey rectangles the distribution of the first two quartiles around the median. (**C**) Comparison of cross-correlogram profiles (i.e. after compressing extreme values) between neurons of the same tetrodes or other tetrodes (see 'Materials and methods' section). *Left*, log Mahalanobis distance from each neuron to all other neurons from the same tetrodes and average distance to tetrodes on other hybrid electrodes. Black circles and vertical lines on the sides show average and SD, respectively. *Right*, Same as *left* but within tetrode distance in comparison to average distance to tetrodes from the same hybrid. Colour of each neuron indicates hybrid electrode of origin, as in **B**.

Neural dynamics specific to FR that are not exclusively related to IED

To ensure that the pattern of neural dynamics is specific to FRs and not to IEDs *per se*, we have analysed three subjects (Subjects 1, 2 and 8) who showed convincing IEDs with neuronal activity on several tetrodes and without FRs (Supplementary Fig. 3). IEDs without FR were associated with a similar discharge pattern in local networks as for FRs: peak discharge followed by inhibition, which were much stronger overall than the effect on distal electrodes (i.e. global networks). However, the effect of IEDs without any FR was much smaller in local networks than for FRs. Both peak and post-event inhibition were stronger for FRs than for IEDs without any FR. Furthermore, no noticeable inhibition was observed after IEDs without any FR in global networks, unlike after FRs.

Discussion

Unravelling the neuronal basis of epileptic activity is a crucial step towards the development of new and potentially patient-specific diagnostic and therapeutic strategies. To this end, accurate recordings of multiple single units at various anatomical scales is crucial. Decades of animal research has pointed to the advantages of polytrode recordings, especially with tetrodes, to separate extracellular waveforms of multiple single units.[43,44] Here, by using new hybrid electrodes containing 2–3 tetrodes implanted intracranially in epileptic patients, we characterized some fundamental aspects of neuronal dynamics during interictal discharge (Fig. 2). Specifically, we demonstrated that FRs were associated with increased neuronal activity in the local network but not in remote anatomical locations (Fig. 3). In contrast, FRs were followed by neuronal inhibition in brain-wide networks. Neuronal modulation by FRs were homogeneous in local networks but differed across hybrid electrodes (i.e. brain areas), even in the same subjects (Fig. 4). Finally, FRs were followed by periods of decreased firing that were circuit-specific and closely related to the inter-FR intervals (Fig. 5). This post-FR inhibition was directly related to the shape of the IED in the LFP (Fig. 6). These findings shed light on the neuronal mechanism underlying interictal activity generation, as well as

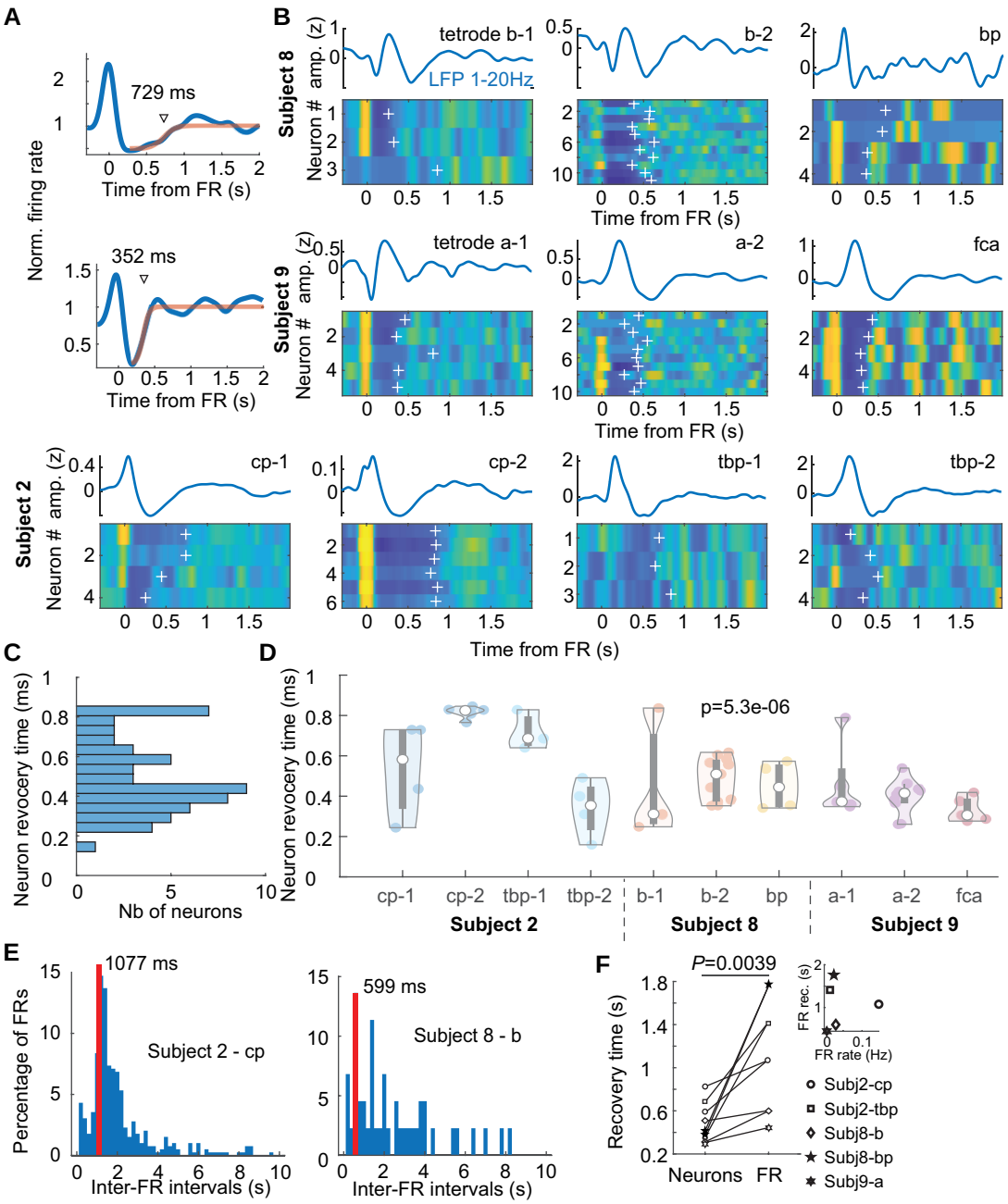

Figure 5 Post-FR recovery of local network states. (**A**) Identification of post-FR neuronal recovery time by fitting post-FR neuronal cross-correlograms with sigmoids. Cross-correlograms are normalized to the neuron's session-wide average firing rate. (**B**) Tetrode-by-tetrode post-FR neuronal cross-correlograms in three subjects (total of 6 hybrid electrodes and 55 units with a significant sigmoid fit in the 50–1500 ms range). White crosses indicate recovery time (obtained as in **A**). (**C**) Distribution of neuronal recovery time in three subjects. (**D**) Distribution of tetrode-by-tetrode recovery times (same presentation as in Fig. 4B). (**E**) Inter-FR interval distribution from two hybrid electrodes (two subjects). (**F**) Hybrid-by-hybrid neuronal and FR recovery times. Inset, FR recovery time as a function of FR occurrence rate ($r = 0.06$; $P = 0.9$; Pearson's correlation).

on the mechanism that prevents the propagation of epileptiform activity and thereby possibly delaying the progression of the disease.

This study could not address some key issues regarding neuronal and epileptiform activity in subjects. First, the recordings were limited in time and could only focus on interictal discharges. How the neuronal dynamics during FRs are related to ictal discharges remains unknown. Next, the number of subjects included in this study was too limited to explore the precise link between neuronal dynamics during FRs and anatomy, that is, potential differences in neuronal firing in different brain areas. Last, the total number of neurons was still too limited to explore potential differences in cell types. However, our data show how neuronal population is organized around FRs across multiple levels, from the local network (<1 mm) to brain-wide neuronal interaction.

Our findings point to a local generation of FRs, with the typical radius of FR generators being 1–2 mm, confirming previous observations in animal models of epilepsy.[30] Specifically, FRs do not always occur concomitantly on all tetrodes of the same hybrid electrodes. Even if they did, they were not necessarily in phase

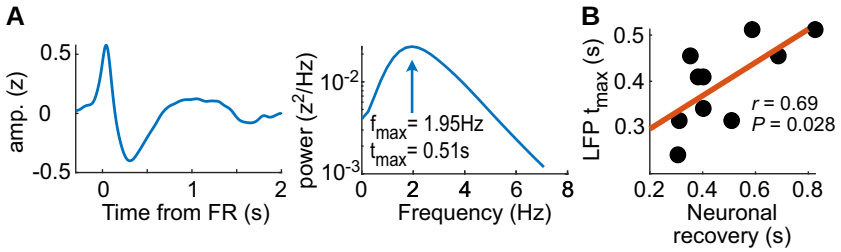

Figure 6 Post-FR recovery of neuronal activity correlates with FR-triggered IED shape. (**A**) *Left*, An example of FR-triggered IED (Subject 2-*cp1*); *right*, power spectrum of the IED, showing a local maximum that determines t_{max}, the typical duration of the IED. (**B**) Typical duration of the IED as a function of post-FR neuronal recovery time.

(Fig. 1). Furthermore, the transient and synchronous increase in neuronal firing at the time of FRs in the local circuits suggests that FRs are generated by the firing of neuronal ensembles in the vicinity of the electrode showing FRs (Figs. 2–4), as is the case for physiological ripples in rodents.[68] The level of excitation at the time of FRs can vary significantly across the tetrodes of a single hybrid electrode (Fig. 4). This observation may be due to differences in recording location, e.g. cortical layers, and additional recordings will be necessary to precisely understand the origin of this difference. At any rate, the proposed size of FR generators is consistent with human anatomical data (e.g. the typical size of cortical neuronal processes)[69] and the spatial extent of neuronal pairwise coordination in the neocortex.[70]

The signals recorded on macro-contacts represent the summation of LFPs in a much larger volume than tetrode micro-wires. The presence of FRs on macro-contacts could therefore mean two things: that a large portion of tissue around the macro-contact generates FRs with random phases, or that a smaller volume generates FRs that are precisely in phase.[59] In general, however, fewer FRs are detected with macroelectrodes than micro-electrodes. The ratio of FRs recorded in the seizure-onset zone to FRs in non-seizure-onset zones is higher for micro-electrodes than for macroelectrodes.[29] In some cases, FRs can be recorded exclusively in the EZ by micro-electrodes (especially tetrodes), while none can be detected on the macroelectrodes.[46] These observations are in line with our findings that FR generators are certainly of limited anatomical size. LFPs recorded on micro-wires therefore provide key insights into the dynamics of the local tissue, potentially providing information on the origin of the disorder.[71]

The transient increase in neuronal firing during FRs in local networks is followed by a suppression of neuronal activity (Figs 3–5). This is probably the result of inhibitory neuron recruitment by FRs, as observed in rodents *in vitro*[72] and *in vivo* after physiological ripples[32,34] and FRs.[73] This could also be the consequence of a transition to 'down' states,[3] that is, the transient suppression of all synaptic and spiking activity in thalamocortical networks. Similar observations have been obtained from human resected tissue.[74] The suppression of neuronal activity after FRs was slow (200–800 ms; Fig. 5), suggesting that this effect may be mediated, at least in part, by slow GABA receptors, such as GABAB. The range of these time constants is consistent with *in vitro* studies.[72,74] The inter-tetrode variance of the neuronal recovery duration could be due to several factors, such as different synaptic dynamics, neuronal excitability and network connectivity,[72,75] but the precise mechanism remains to be elucidated.

Functionally, the decrease in neuronal activity following FRs delays the occurrence of the next FR when the network is particularly excitable, which acts as a refractory period for the network[32,72,76-78]. In fact, the typical minimal duration between two consecutive FRs was always longer that the duration of activity suppression. And yet the timescales of neuronal spiking and FR recovery (i.e. time to reach baseline occurrence rate) were of the same order of magnitude and specific to each local network, even within the same subject (Fig. 5), which demonstrates a link between fine-tuned neuronal dynamics and network-level events. Neuronal and FR recovery rate were not significantly correlated *per se*, which is partially due to the limited number of observations. However, this also supports the idea that recovery and neuronal activity is only one of several processes leading to the generation of another population burst.[72] It has been suggested that inhibition-induced refractoriness in local networks plays a critical role in the propagation of interictal discharge across areas[79] and future work will unravel this phenomenon at the neuronal level.

IEDs can have highly variable spatiotemporal profiles,[80] as seen for example on two neighbouring tetrodes in Fig. 2A. Here, we have shown that neuronal response to FRs was network-specific in terms of excitation level, overall temporal profile of neuronal modulation, and post-FR firing inhibition, which confirms earlier reports of high variability in neuronal responses to IEDs.[39,40] Our results also indicate that these network properties are specific to IEDs associated with FRs, compared to IEDs devoid of FR. Such network specificity is also consistent with reports of different single-cell dynamics during oscillations in the ripple band (~200 Hz) depending on whether they are associated with an IED or a preictal discharge.[81] Therefore, different mechanisms may underlie the generation of IEDs and FRs.[82] Further investigation of the precise relationship between local neuronal activity and associated events in the LFP (IED with or without FRs) will be necessary to guide future clinical investigation of epileptic tissue with IED and IED-concurrent FRs.

The multi-hybrid electrode implants allowed us to address the question of the long-range coordination of neuronal activity during FRs. The high excitation associated with FRs must have consequences in networks beyond the local circuits where FRs are generated,[83] as seen, for example, in the cortex after hippocampal ripples in rodents.[84–86] However, in general, neurons in other brain areas show no increased excitation during FRs (Fig. 3). In contrast, neuronal activity tends to be globally suppressed after FRs (Fig. 3). Although the level of activity suppression is lower than the level observed locally (i.e. after FRs in the local circuit), this observation begs the question of the underlying anatomical pathway mediating this long-range activity suppression. One possibility is that this effect is mediated by feedforward inhibition akin to the strong recruitment of fast-spiking inhibitory neurons after hippocampal ripples in rodents.[87] Importantly, feedforward inhibition has been suggested to be a key mechanism that controls the spread of the ictal wavefront.[88–90] Another possibility is that post-FR activity

suppression is mediated by long-range inhibitory neurons.[91,92] Long-range activity suppression may also be due to an indirect network effect, for example, through cortico-thalamo-cortical pathways. This is supported by the triggering of specific thalamo-cortical oscillations by physiological ripples[87,93] and by IEDs in rodents and human subjects.[3] Further work will be necessary to investigate the relationship between FR-triggered long-range activity suppression and the precise anatomical pathway of generalized ictal activity.

The global decrease in neuronal activity following FRs indicates that, although the underlying generators are small, FRs have a widespread impact on brain activity. We showed that FRs are followed by neuronal activity inhibition in large-scale brain networks, including healthy tissues. These findings suggest that localized pathological neuronal dynamics impact even healthy tissue. This reveals how even localized pathological brain dynamics can impair normal brain functions. Epilepsy is a debilitating brain disorder associated with cognitive impairment, especially when it no longer responds to antiseizure drugs.[94] This interruption of normal brain activity (especially because of the preferential occurrence of FRs during sleep,[95] but also in periods of rest during wakefulness as our results demonstrated) may certainly play a role in cognitive impairment, deficits that have been connected to the occurrence of IEDs[1,3–5] and, more recently, directly to FR.[2,6]

In conclusion, the new hybrid electrodes used in the present study offer unique access to the neuronal dynamics underlying epileptiform activity. Tetrodes enable the characterization of neuronal activity in micro- and macro-circuits. By detecting more local FR generators, combining tetrodes to macroelectrodes in clinical routine could more accurately define the extent of the EZ and improve confidence in the outcome of neurosurgery. Furthermore, understanding the generation and long-range consequences of FRs will shed light on the mechanisms underlying cognitive impairment in epilepsy.

Acknowledgements

We thank Ludovic Gardy for his help in data acquisition and in the quantification of FR properties; Karine Bouyer, Simona Celebrini, Pascale Cook, Martin Deudon, Leila Reddy, Simon J. Thorpe, for helpful comments and help with data acquisition; Konstantinos Niasotis for working on the data analysis pipeline; Sara Mahallati, Adrian Duszkiewicz and Karim Benchenane for discussing and commenting on an earlier version of the manuscript.

Funding

This project was made possible with the financial support of the European Research Council (under the European Union's Seventh Framework Programme (FP/2007-2013)/ERC grant agreement no. 323711, M4 project), the Fondation Française pour la Recherche sur l'Epilepsie (Prix Marion Clignet), Toulouse University Hospital (through a call for technological and organization innovation research projects) and Health Canada (through the Canada Brain Research Fund), an innovative partnership between the government of Canada (through Health Canada), and Brain Canada (to A.P.). This work was also supported by a Canadian Institutes for Health Research Project Grant (PJT-155957), an Natural Sciences and Engineering Research Council Discovery Grant (RGPIN-2018-04600) and a Canada-Israel Health Research Initiative, jointly funded by the Canadian Institutes of Health Research, the Israel Science Foundation, the International Development Research Centre, Canada and the Azrieli Foundation (108877-001) to A.P., as well as a fellowship from the Ligue Française Contre l'Epilepsie to J.C.

Competing interests

The authors report no competing interests.

Supplementary material

Supplementary material is available at *Brain* online.

References

1. Binnie CD. Cognitive impairment during epileptiform discharges: Is it ever justifiable to treat the EEG? *Lancet Neurol*. 2003;2:725-730.
2. Ewell LA, Fischer KB, Leibold C, Leutgeb S, Leutgeb JK. The impact of pathological high-frequency oscillations on hippocampal network activity in rats with chronic epilepsy. *eLife*. 2019;8:e42148.
3. Gelinas JN, Khodagholy D, Thesen T, Devinsky O, Buzsáki G. Interictal epileptiform discharges induce hippocampal-cortical coupling in temporal lobe epilepsy. *Nat Med*. 2016;22:641-648.
4. Holmes GL, Lenck-Santini PP. Role of interictal epileptiform abnormalities in cognitive impairment. *Epilepsy Behav*. 2006;8:504-515.
5. Lambert I, Tramoni-Negre E, Lagarde S, *et al*. Hippocampal interictal spikes during sleep impact long-term memory consolidation. *Ann Neurol*. 2020;87:976-987.
6. Sun D, van 't Klooster MA, van Schooneveld MMJ, *et al*. High frequency oscillations relate to cognitive improvement after epilepsy surgery in children. *Clin Neurophysiol*. 2020;131:1134-1141.
7. Bartolomei F, Lagarde S, Wendling F, *et al*. Defining epileptogenic networks: Contribution of SEEG and signal analysis. *Epilepsia*. 2017;58:1131-1147.
8. Bragin A, Engel J, Wilson CL, Fried I, Buzsáki G. High-frequency oscillations in human brain. *Hippocampus*. 1999;9:137-142.
9. Bragin A, Engel J, Wilson CL, Fried I, Mathern GW. Hippocampal and entorhinal cortex high-frequency oscillations (100–500 Hz) in human epileptic brain and in kainic acid-treated rats with chronic seizures. *Epilepsia*. 1999;40:127-137.
10. Urrestarazu E, Chander R, Dubeau F, Gotman J. Interictal high-frequency oscillations (100–500 Hz) in the intracerebral EEG of epileptic patients. *Brain*. 2007;130:2354-2366.
11. van 't Klooster MA, van Klink NEC, Leijten FSS, *et al*. Residual fast ripples in the intraoperative corticogram predict epilepsy surgery outcome. *Neurology*. 2015;85:120-128.
12. van Klink NEC, van't Klooster MA, Zelmann R, *et al*. High frequency oscillations in intra-operative electrocorticography before and after epilepsy surgery. *Clin Neurophysiol*. 2014;125:2212-2219.
13. Zijlmans M, Jiruska P, Zelmann R, Leijten FSS, Jefferys JGR, Gotman J. High-frequency oscillations as a new biomarker in epilepsy. *Ann Neurol*. 2012;71:169-178.
14. Jacobs J, Zijlmans M, Zelmann R, *et al*. High-frequency electroencephalographic oscillations correlate with outcome of epilepsy surgery. *Ann Neurol*. 2010;67:209-220.
15. Wu JY, Sankar R, Lerner JT, Matsumoto JH, Vinters HV, Mathern GW. Removing interictal fast ripples on electrocorticography linked with seizure freedom in children. *Neurology*. 2010;75:1686-1694.

16. Lévesque M, Avoli M. High-frequency oscillations and focal seizures in epileptic rodents. *Neurobiol Dis*. 2019;124:396-407.
17. Ryvlin P, Cross JH, Rheims S. Epilepsy surgery in children and adults. *Lancet Neurol*. 2014;13:1114-1126.
18. Rosenow F, Lüders H. Presurgical evaluation of epilepsy. *Brain*. 2001;124:1683-1700.
19. Akiyama T, McCoy B, Go CY, *et al*. Focal resection of fast ripples on extraoperative intracranial EEG improves seizure outcome in pediatric epilepsy. *Epilepsia*. 2011;52:1802-1811.
20. Fedele T, van 't Klooster M, Burnos S, *et al*. Automatic detection of high frequency oscillations during epilepsy surgery predicts seizure outcome. *Clin Neurophysiol*. 2016;127:3066-3074.
21. Haegelen C, Perucca P, Châtillon CE, *et al*. High-frequency oscillations, extent of surgical resection, and surgical outcome in drug-resistant focal epilepsy. *Epilepsia*. 2013;54:848-857.
22. Nevalainen P, von Ellenrieder N, Klimeš P, Dubeau F, Frauscher B, Gotman J. Association of fast ripples on intracranial EEG and outcomes after epilepsy surgery. *Neurology*. 2020;95:e2235-e2245.
23. Jacobs J, Wu JY, Perucca P, *et al*. Removing high-frequency oscillations: A prospective multicenter study on seizure outcome. *Neurology*. 2018;91:e1040-e1052.
24. Roehri N, Pizzo F, Lagarde S, *et al*. High-frequency oscillations are not better biomarkers of epileptogenic tissues than spikes. *Ann Neurol*. 2018;83:84-97.
25. Blanco JA, Stead M, Krieger A, *et al*. Data mining neocortical high-frequency oscillations in epilepsy and controls. *Brain*. 2011;134:2948-2959.
26. Kondylis ED, Wozny TA, Lipski WJ, *et al*. Detection of high-frequency oscillations by hybrid depth electrodes in standard clinical intracranial EEG recordings. *Front Neurol*. 2014;5:149.
27. Ogren JA, Wilson CL, Bragin A, *et al*. Three-dimensional surface maps link local atrophy and fast ripples in human epileptic hippocampus. *Ann Neurol*. 2009;66:783-791.
28. Weiss SA, Staba R, Bragin A, *et al*. Interneurons and principal cell firing in human limbic areas at focal seizure onset. *Neurobiol Dis*. 2019;124:183-188.
29. Worrell GA, Gardner AB, Stead SM, *et al*. High-frequency oscillations in human temporal lobe: Simultaneous microwire and clinical macroelectrode recordings. *Brain*. 2008;131:928-937.
30. Bragin A, Mody I, Wilson CL, Engel J. Local generation of fast ripples in epileptic brain. *J Neurosci*. 2002;22:2012-2021.
31. Buzsaki G, Horvath Z, Urioste R, Hetke J, Wise K. High-frequency network oscillation in the hippocampus. *Science*. 1992:256:1025-1027.
32. English DF, Peyrache A, Stark E, *et al*. Excitation and inhibition compete to control spiking during hippocampal ripples: Intracellular study in behaving mice. *J Neurosci*. 2014;34:16509-16517.
33. Gan J, Weng SM, Pernía-Andrade AJ, Csicsvari J, Jonas P. Phase-locked inhibition, but not excitation, underlies hippocampal ripple oscillations in awake mice in vivo. *Neuron*. 2017;93:308-314.
34. Hulse BK, Moreaux LC, Lubenov EV, Siapas AG. Membrane potential dynamics of CA1 pyramidal neurons during hippocampal ripples in awake mice. *Neuron*. 2016;89:800-813.
35. Stark E, Roux L, Eichler R, Senzai Y, Royer S, Buzsáki G. Pyramidal cell-interneuron interactions underlie hippocampal ripple oscillations. *Neuron*. 2014;83:467-480.
36. Valero M, Averkin RG, Fernandez-Lamo I, *et al*. Mechanisms for selective single-cell reactivation during offline sharp-wave ripples and their distortion by fast ripples. *Neuron*. 2017;94:1234-1247.e7.
37. Ylinen A, Bragin A, Nadasdy Z, *et al*. Sharp wave-associated high-frequency oscillation (200 Hz) in the intact hippocampus: Network and intracellular mechanisms. *J Neurosci*. 1995;15:30-46.
38. Cash SS, Hochberg LR. The emergence of single neurons in clinical neurology. *Neuron*. 2015;86:79-91.
39. Alarcón G, Martinez J, Kerai SV, *et al*. In vivo neuronal firing patterns during human epileptiform discharges replicated by electrical stimulation. *Clin Neurophysiol*. 2012;123:1736-1744.
40. Keller CJ, Truccolo W, Gale JT, *et al*. Heterogeneous neuronal firing patterns during interictal epileptiform discharges in the human cortex. *Brain*. 2010;133:1668-1681.
41. Paulk AC, Kfir Y, Khanna AR, *et al*. Large-scale neural recordings with single neuron resolution using neuropixels probes in human cortex. *Nat Neurosci*. Published online 31 January 2022.
42. Despouy E, Curot J, Reddy L, *et al*. Recording local field potential and neuronal activity with tetrodes in epileptic patients. *J Neurosci Methods*. 2020;341:108759.
43. Gray CM, Maldonado PE, Wilson M, McNaughton B. Tetrodes markedly improve the reliability and yield of multiple single-unit isolation from multi-unit recordings in cat striate cortex. *J Neurosci Methods*. 1995;63:43-54.
44. Harris KD, Henze DA, Csicsvari J, Hirase H, Buzsáki G. Accuracy of tetrode spike separation as determined by simultaneous intracellular and extracellular measurements. *J Neurophysiol*. 2000;84:401-414.
45. Isnard J, Taussig D, Bartolomei F, *et al*. French guidelines on stereoelectroencephalography (SEEG). *Neurophysiol Clin*. 2018;48:5-13.
46. Despouy E, Curot J, Denuelle M, *et al*. Neuronal spiking activity highlights a gradient of epileptogenicity in human tuberous sclerosis lesions. *Clin Neurophysiol*. 2019;130:537-547.
47. Talairach J, Bancaud J, Bonis A, Szikla G, Tournoux P. Functional stereotaxic exploration of epilepsy. *Stereotact Funct Neurosurg*. 1962;22:328-331.
48. Zijlmans M, Worrell GA, Dümpelmann M, *et al*. How to record high-frequency oscillations in epilepsy: A practical guideline. *Epilepsia*. 2017;58:1305-1315.
49. Nasiotis K, Cousineau M, Tadel F, *et al*. Integrated open-source software for multiscale electrophysiology. *Sci Data*. 2019;6:231.
50. Yger P, Spampinato GL, Esposito E, *et al*. A spike sorting toolbox for up to thousands of electrodes validated with ground truth recordings in vitro and in vivo. *eLife*. 2018;7:e34518.
51. Hill DN, Mehta SB, Kleinfeld D. Quality metrics to accompany spike sorting of extracellular signals. *J Neurosci*. 2011;31:8699-8705.
52. Hazan L, Zugaro M, Buzsáki G. Klusters, NeuroScope, NDManager: A free software suite for neurophysiological data processing and visualization. *J Neurosci Methods*. 2006;155:207-216.
53. Zelmann R, Zijlmans M, Jacobs J, Châtillon CE, Gotman J. Improving the identification of high frequency oscillations. *Clin Neurophysiol*. 2009;120:1457-1464.
54. Jacobs J, LeVan P, Chander R, Hall J, Dubeau F, Gotman J. Interictal high-frequency oscillations (80–500 Hz) are an indicator of seizure onset areas independent of spikes in the human epileptic brain. *Epilepsia*. 2008;49:1893-1907.
55. Bénar CG, Chauvière L, Bartolomei F, Wendling F. Pitfalls of high-pass filtering for detecting epileptic oscillations: A technical note on "false" ripples. *Clin Neurophysiol*. 2010;121:301-310.
56. Roehri N, Lina JM, Mosher JC, Bartolomei F, Bénar CG. Time-frequency strategies for increasing high-frequency oscillation detectability in intracerebral EEG. *IEEE Trans Biomed Eng*. 2016;63:2595-2606.
57. Colombet B, Woodman M, Badier JM, Bénar CG. Anywave: A cross-platform and modular software for visualizing and

processing electrophysiological signals. *J Neurosci Methods*. 2015; 242:118-126.
58. Tadel F, Baillet S, Mosher JC, Pantazis D, Leahy RM. Brainstorm: A user-friendly application for MEG/EEG analysis. *Comput Intell Neurosci*. 2011;2011:879716.
59. Ibarz JM, Foffani G, Cid E, Inostroza M, Menendez de la Prida L. Emergent dynamics of fast ripples in the epileptic hippocampus. *J Neurosci*. 2010;30:16249-16261.
60. Smith EH, Merricks EM, Liou JY, *et al*. Dual mechanisms of ictal high frequency oscillations in human rhythmic onset seizures. *Sci Rep*. 2020;10:19166.
61. Kahane P, Landré E, Minotti L, Francione S, Ryvlin P. The Bancaud and Talairach view on the epileptogenic zone: A working hypothesis. *Epileptic Disord Int Epilepsy J Videotape*. 2006;8:S16-S26.
62. Lüders H, Schuele SU. Epilepsy surgery in patients with malformations of cortical development. *Curr Opin Neurol*. 2006;19:169-174.
63. de Curtis M, Avanzini G. Interictal spikes in focal epileptogenesis. *Prog Neurobiol*. 2001;63:541-567.
64. Talairach J, Bancaud J. Lesion, "irritative" zone and epileptogenic focus. *Stereotact Funct Neurosurg*. 1966;27:91-94.
65. Mathis A, Mamidanna P, Cury KM, *et al*. Deeplabcut: Markerless pose estimation of user-defined body parts with deep learning. *Nat Neurosci*. 2018;21:1281-1289.
66. Viejo G, Peyrache A. Precise coupling of the thalamic head-direction system to hippocampal ripples. *Nat Commun*. 2020; 11:2524.
67. Buzsáki G, Mizuseki K. The log-dynamic brain: How skewed distributions affect network operations. *Nat Rev Neurosci*. 2014;15: 264-278.
68. Schomburg EW, Anastassiou CA, Buzsáki G, Koch C. The spiking component of oscillatory extracellular potentials in the rat hippocampus. *J Neurosci*. 2012;32:11798-11811.
69. Braitenberg V, Schüz A. *Cortex: Statistics and geometry of neuronal connectivity*. Springer; 1998.
70. Peyrache A, Dehghani N, Eskandar EN, *et al*. Spatiotemporal dynamics of neocortical excitation and inhibition during human sleep. *Proc Natl Acad Sci U S A*. 2012;109:1731-1736.
71. Schevon CA, Tobochnik S, Eissa T, *et al*. Multiscale recordings reveal the dynamic spatial structure of human seizures. *Neurobiol Dis*. 2019;127:303-311.
72. Menendez de la Prida L, Huberfeld G, Cohen I, Miles R. Threshold behavior in the initiation of hippocampal population bursts. *Neuron*. 2006;49:131-142.
73. Muldoon SF, Villette V, Tressard T, *et al*. GABAergic inhibition shapes interictal dynamics in awake epileptic mice. *Brain*. 2015;138:2875-2890.
74. Cohen I, Navarro V, Clemenceau S, Baulac M, Miles R. On the origin of interictal activity in human temporal lobe epilepsy *in vitro*. *Science*. 2002;298:1418-1421.
75. Levenstein D, Buzsáki G, Rinzel J. NREM sleep in the rodent neocortex and hippocampus reflects excitable dynamics. *Nat Commun*. 2019;10:2478.
76. de Curtis M, Jefferys JGR, Avoli M. Interictal epileptiform discharges in partial epilepsy: complex neurobiological mechanisms based on experimental and clinical evidence. In: Noebels JL Avoli M Rogawski MA Olsen RW and Delgado-Escueta AV, eds. *Jasper's basic mechanisms of the epilepsies*. 4th edn. National Center for Biotechnology Information (US); 2012. Accessed 1 July 2021. http://www.ncbi.nlm.nih.gov/books/NBK98179/
77. Miles R, Wong RKS. Single neurones can initiate synchronized population discharge in the hippocampus. *Nature*. 1983;306: 371-373.
78. Prince DA. The depolarization shift in "epileptic" neurons. *Exp Neurol*. 1968;21:467-485.
79. Sabolek HR, Swiercz WB, Lillis KP, *et al*. A candidate mechanism underlying the variance of interictal spike propagation. *J Neurosci*. 2012;32:3009-3021.
80. Alarcon G, Guy CN, Binnie CD, Walker SR, Elwes RD, Polkey CE. Intracerebral propagation of interictal activity in partial epilepsy: Implications for source localisation. *J Neurol Neurosurg Psychiatry*. 1994;57:435-449.
81. Alvarado-Rojas C, Lehongre K, Bagdasaryan J, *et al*. Single-unit activities during epileptic discharges in the human hippocampal formation. *Front Comput Neurosci*. 2013;7:140. Accessed 28 June 2022. https://www.frontiersin.org/article/10.3389/fncom.2013.00140
82. Demont-Guignard S, Benquet P, Gerber U, Biraben A, Martin B, Wendling F. Distinct hyperexcitability mechanisms underlie fast ripples and epileptic spikes. *Ann Neurol*. 2012;71:342-352.
83. González Otárula KA, von Ellenrieder N, Cuello-Oderiz C, Dubeau F, Gotman J. High-frequency oscillation networks and surgical outcome in adult focal epilepsy. *Ann Neurol*. 2019;85:485-494.
84. Karimi Abadchi J, Nazari-Ahangarkolaee M, Gattas S, *et al*. Spatiotemporal patterns of neocortical activity around hippocampal sharp-wave ripples. *eLife*. 2020;9:e51972.
85. Khodagholy D, Gelinas JN, Buzsáki G. Learning-enhanced coupling between ripple oscillations in association cortices and hippocampus. *Science*. 2017;358:369-372.
86. Peyrache A, Khamassi M, Benchenane K, Wiener SI, Battaglia FP. Replay of rule-learning related neural patterns in the prefrontal cortex during sleep. *Nat Neurosci*. 2009;12:919-926.
87. Peyrache A, Battaglia FP, Destexhe A. Inhibition recruitment in prefrontal cortex during sleep spindles and gating of hippocampal inputs. *Proc Natl Acad Sci USA*. 2011;108:17207-17212.
88. Smith EH, Liou JY, Davis TS, *et al*. The ictal wavefront is the spatiotemporal source of discharges during spontaneous human seizures. *Nat Commun*. 2016;7:11098.
89. Shamas M, Benquet P, Merlet I, *et al*. On the origin of epileptic high frequency oscillations observed on clinical electrodes. *Clin Neurophysiol*. 2018;129:829-841.
90. Trevelyan AJ, Sussillo D, Watson BO, Yuste R. Modular propagation of epileptiform activity: evidence for an inhibitory veto in neocortex. *J Neurosci*. 2006;26:12447-12455.
91. Jinno S, Klausberger T, Marton LF, *et al*. Neuronal diversity in GABAergic long-range projections from the hippocampus. *J Neurosci*. 2007;27:8790-8804.
92. Tomioka R, Okamoto K, Furuta T, *et al*. Demonstration of long-range GABAergic connections distributed throughout the mouse neocortex. *Eur J Neurosci*. 2005;21:1587-1600.
93. Siapas AG, Wilson MA. Coordinated interactions between hippocampal ripples and cortical spindles during slow-wave sleep. *Neuron*. 1998;21:1123-1128.
94. Tramoni E, Felician O, Barbeau EJ, *et al*. Long-term consolidation of declarative memory: insight from temporal lobe epilepsy. *Brain*. 2011;134:816-831.
95. Bagshaw AP, Jacobs J, LeVan P, Dubeau F, Gotman J. Effect of sleep stage on interictal high-frequency oscillations recorded from depth macroelectrodes in patients with focal epilepsy. *Epilepsia*. 2009;50:617-628.